





Review

# Neil Gehrels–Swift Observatory’s Ultraviolet/Optical Telescope Observations of Small Bodies in the Solar System

Dennis Bodewits <sup>1,\*</sup>, Zexi Xing <sup>1,2</sup>, Mohammad Saki <sup>1</sup> and Jeffrey P. Morgenthaler <sup>3</sup><sup>1</sup> Department of Physics, Edmund C. Leach Science Center, Auburn University, Auburn, AL 38642, USA<sup>2</sup> Department of Physics and Laboratory for Space Research, The University of Hong Kong, Pokfulam Road, Hong Kong, China<sup>3</sup> Planetary Science Institute, 1700 E. Fort Lowell, Suite 106, Tucson, AZ 85719, USA

\* Correspondence: dennis@auburn.edu

**Abstract:** The *Neil–Gehrels Swift Observatory* has added extensively to our understanding of small bodies in our solar system through its capabilities to rapidly respond to short-live events such as outbursts and collisions, through its near-ultraviolet coverage, and by its ability to track time-dependent changes through monitoring campaigns. These capabilities have enabled many significant studies, including the onset and evolution of different sources of water in comet C/2009 P1 (Garradd), the unprecedented changes in the rotation period of comet 41P/Tuttle–Giacobini–Kresák, near-UV spectroscopic observations of asteroids that can help us understand how their properties evolve over time, and the first observations of the aftermath of a collision between a 100 m sized asteroid and the large primitive asteroid 596 (Scheila). In this review paper, we will highlight some of the observational results of *Swift*-UVOT in the field of small-body research.

**Keywords:** comets; asteroids; near ultraviolet astronomy



**Citation:** Bodewits, D.; Xing, Z.; Saki, M.; Morgenthaler, J.P. Neil Gehrels–Swift Observatory’s Ultraviolet/Optical Telescope Observations of Small Bodies in the Solar System. *Universe* **2023**, *9*, 78. <https://doi.org/10.3390/universe9020078>

Academic Editors: Peter Roming and Michael Siegel

Received: 22 December 2022

Revised: 18 January 2023

Accepted: 24 January 2023

Published: 31 January 2023



**Copyright:** © 2023 by the authors. Licensee MDPI, Basel, Switzerland. This article is an open access article distributed under the terms and conditions of the Creative Commons Attribution (CC BY) license (<https://creativecommons.org/licenses/by/4.0/>).

## 1. Introduction

Small bodies in our solar system are considered leftovers from the era of planet formation that contain significant reservoirs of organics and volatiles [1–3]. The small bodies encompass multiple groups of diverse objects, such as comets, asteroids, Centaurs, Trojans, etc. Those groups are loosely defined by their orbital and physical properties. For example, Jupiter family comets are objects with specific dynamical relation to Jupiter (Tisserand parameter < 3) that show sublimation activity. Most asteroids are found in the Main Belt, between the orbits of Jupiter and Mars, with a Tisserand parameter > 3. Traditionally, comets are considered volatile-rich and asteroids “dry”. We now know that these separations are not this simple. For example, there are several objects in the Main Belt that show repeated evidence of sublimation activity, such as 133P/Elst-Pizarro and 238P/Read [4]. Many of these objects seem to be dynamically stable in the Main Belt, ruling out that they are cometary interlopers. Not all asteroids that grow a tail or dusty coma are sublimating ice; disruptions such as rotational fragmentation and impacts can loft material from the surface [5,6]. On the other side of the spectrum, the results of the *Rosetta* mission to 67P/Churyumov–Gerasimenko suggest that comets might contain much less ice than previously assumed, with estimated refractory-to-ice mass ratios in the nucleus between 0.2 and 7 [7]. The discovery of objects on comet-like trajectories that show no evidence of activity (Manx comets and asteroids on cometary orbits (ACOs) [8,9]) suggests that there are either asteroidal, purely rocky objects in the Oort cloud, or that comets can effectively devolatilize thermally accessible ice and survive intact. To interpret the information that small bodies can provide us on the conditions of the disk from which they formed, to better understand their role in the delivery of volatiles and organic molecules to the inner solar

system, and to assess what resources they can provide it is critical to understand how small bodies evolve through, and because of, activity.

The *Neil Gehrels–Swift observatory* was designed for rapid follow-up of gamma-ray bursts [10]. It is equipped with three bore-sighted instruments covering gamma rays, X-rays, and UV-optical wavelengths. Its Ultraviolet/Optical Telescope (UVOT, [11]) is a modified Ritchey–Chrétien telescope with a diameter of 30 cm. It has pixels that each span 0.502 arcsec over a field of view of 17' × 17', with a point spread function of 2.5". Seven broadband filters allow color discrimination, and two grisms provide low-resolution spectroscopy ( $R \approx 100$  for point sources) at UV (1700–5000 Å) and optical wavelengths (2850–6600 Å) [12–14]. UVOT is equipped with a photon-counting detector, which results in very low background levels but has the disadvantage that, when it is at high incident fluxes ( $>0.01$  counts/s/pixel), coincidence loss—the arrival of more than one photon in a given pixel during a single readout of the detector—will result in nonlinear behavior of the detector that might require significant corrections [13–15].

Since its launch in 2004, the *Neil Gehrels–Swift observatory* has contributed significantly to the study of small bodies in our solar system. As we will demonstrate in this contribution, this is mostly due to *Swift's* coverage of the ultraviolet and to its operational rapid-follow-up and monitoring capabilities. *Swift/UVOT* has proven to be one of the most capable instruments to detect faint signatures of OH (see Figures 1 and 2). OH is produced directly by the photodissociation of H<sub>2</sub>O, the prime volatile in comets. The main fluorescence band of OH ( $A^2\Sigma^+ - X^2\Pi_i$ ) emits around 3085 Å. At these wavelengths, ground-based observations are hampered by both significant atmospheric extinction and often poor sensitivity of many Charge-coupled Devices (CCDs). UVOT combines UV sensitivity with a large field of view and has proven to be well-suited to image the OH gas and dust distribution around comets (Figure 2), even at large heliocentric distances and/or very low activity levels [16,17]. In addition, *Swift* can often follow a comet through more of its orbit than ground-based telescopes, which are limited by their geographical latitude and day/night variations.

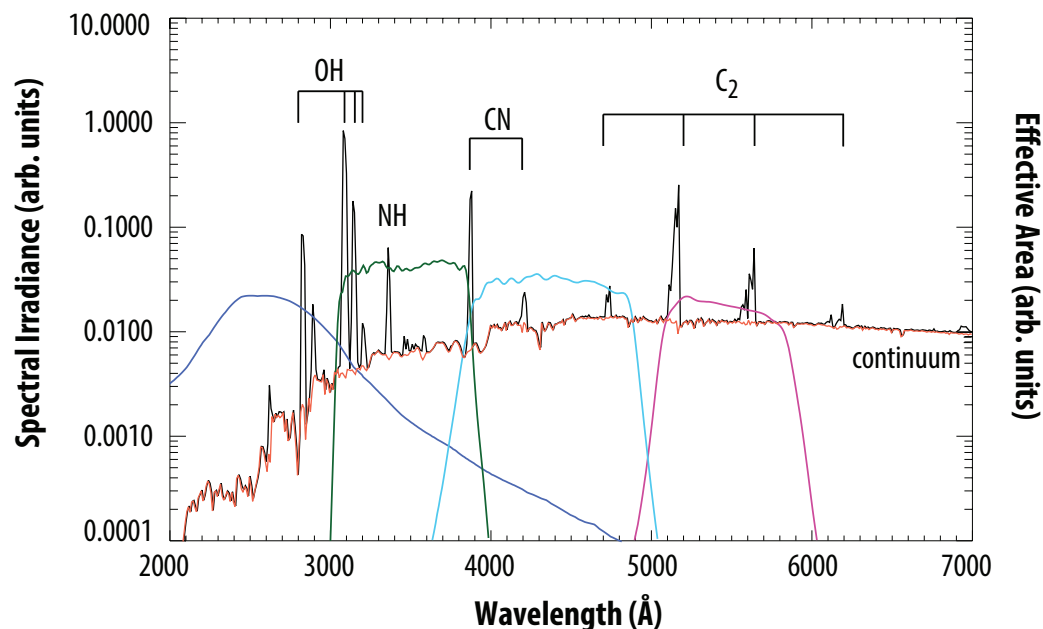


**Figure 1.** Model spectrum of a typical comet generated with the Planetary Spectrum Generator [18]. At near-ultraviolet/optical wavelengths, the cometary spectrum consists of a continuum, caused by sunlight reflected by dust surrounding the nucleus (red), superimposed by the emission features of various radical species, such as OH, CN, and C<sub>2</sub>. Overlaid are the bandpasses of some of UVOT’s filters: UVW1 (blue); U (green); B (cyan); and V (magenta).

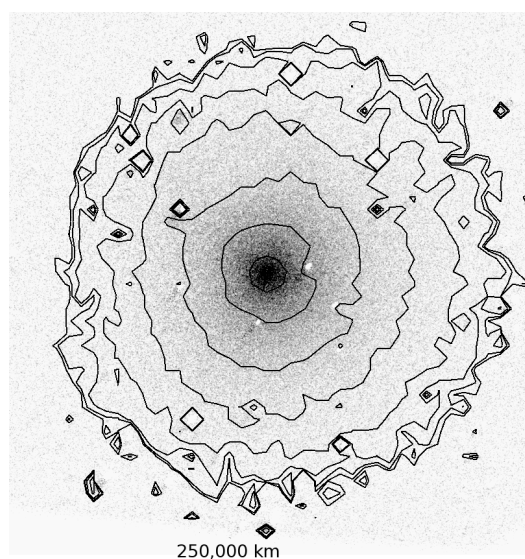


**Figure 2.** *Swift*-UVOT image comet C/2012 K1 (Pan-STARRS) through the UVW1 filter, after continuum removal. A symmetric OH coma of 1 million kilometers across can be seen. The comet was approximately  $V = 11$  mag at the time of the observation.

A lot of small-body science is driven by rapid response and/or target of opportunity observations, which includes confirmation of newly discovered objects, sudden outbursts, collisions between small bodies, and fragmentation events. The brightest comets available are often Long Period Comets from the Oort Cloud, which may or may not have been discovered or sufficiently characterized by the time yearly observing proposals are due. *Swift*'s monitoring capabilities have allowed for unique time domain studies such as the long-term activity evolution of comets on approach and departure from the Sun, seasonal activity changes due to the obliquity of the rotation axis of comet nuclei, and photometric evidence of large changes in their rotation periods. In the next sections, we will present several highlights of *Swift*'s small body observations.

## 2. Highlights

### 2.1. Large Spin-Down of Comet 41P/Tuttle–Giacobini–Kresák

Comet 41P/Tuttle–Giacobini–Kresák made a close approach to Earth in April 2017. Not only did it pass Earth within 0.142 au, but it also was observable for many hours each night from the Northern hemisphere for months. Before the 2017 apparition, 41P was mostly known for its large outbursts in 2005 [19]. In 2017, its geometric conditions allowed for multiple measurements of the comet's rotation period [20–22]. Ground-based observers used comet-specific cyanogen filters to map recurring jets and found a rotation period of 10 h on 7–8 March 2017 UTC [23]. When *Swift* observed 41P between 6–9 May 2017, photometry acquired with UVOT indicated a much longer rotation period of at least 46 h (Figure 3, [20]). This implied that in a time period of only two months, torques caused by the comet's activity decreased its spin rate by more than half. Changes in the rotation of cometary nuclei had been seen before, most notably for *Rosetta*'s 67P/Churyumov–Gerasimenko [24,25], but these changes were tens of minutes at most. *Swift*'s findings suggest that the observed large change in the period of 41P puts it in a distinct evolutionary state as the slow rotation will likely lead to a complete change in its rotational state [20,26].

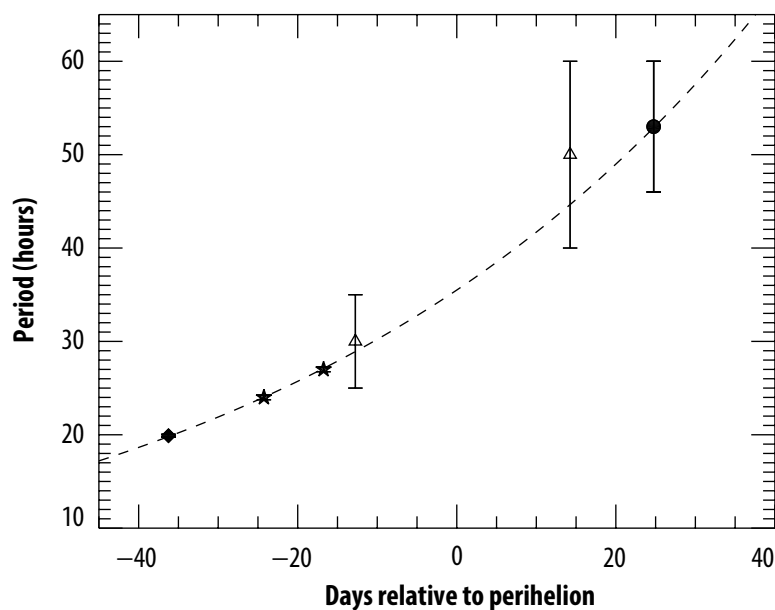


**Figure 3.** The rotation period of comet 41P/Tuttle–Giacobini–Kresák increased from 20 h to over 46 h during its 2017 apparition, the largest change in rotation period ever observed for a comet. These observations suggest that that the comet rapidly evolved into an excited, unstable spin state. Black diamond: Lowell Discovery Telescope [23]; Black stars: Lowell 31" Telescope [27]; open triangles; TRAPPIST [22]; Filled circle: *Swift*/UVOT [20]. The dashed line is drawn to guide the eye, after [20].

## 2.2. Activity Evolution of Comets

Whereas comets are generally considered mixtures of dust and ice, the storage and release of volatiles remain a major topic in comet science [28,29]. This includes questions such as how many volatiles comet nuclei contain [7,30], whether there are significant extended sources in the coma or if all the volatiles are released directly from the nucleus [31–33], and how comets evolve through continued volatile depletion as they age [34]. In addition, studies centered on the chemical composition of comets mostly do so by comparing the abundance of minor species to the water production rate [35]. *Swift*/UVOT has proven to be very sensitive in tracking the fluorescent emission of the OH ( $A^2\Sigma^+ - X^2\Pi_i$ ) band. The OH radical is a direct product of the photodissociation of  $H_2O$  and is therefore commonly used to determine cometary water production rates [36].

The coverage of the OH (A–X) band with the UVW1 filter was first discussed in the interpretation of the UVOT observations of the *Deep Impact* encounter with 9P/Tempel 1 [12]. To assess the continuum contribution to the UVW1 filter, an archival grism spectrum of 73P/Schwassmann–Wachmann 3C was used along with the assumption that comets 9P and 73P had the same OH and dust contributions within the bandpass of UVW1. Later studies used contemporaneous V-band observations to remove the continuum contribution from UVW1 images to create OH maps [16,37], analog to the image processing of narrowband filters [38], with the caveat that the V-band contains emission of the  $C_2$  radical (Figure 1) and that the exact continuum removal factor depends on the color of the dust, which must be either assumed or provided by other observations. Most recently, Xing et al. [17] developed a more sophisticated procedure to remove the continuum contribution from the UVW1 passband by combining theoretical OH column density distributions with observed V-band surface brightness profiles, and by using the color of the dust as a free parameter to identify the best fit.

A good example of the sensitivity of UVOT to OH (A–X) emission was the campaign to characterize the activity evolution of C/2009 P1 (Garradd), between April 2011 and October 2012. *Swift* started observing when the comet was  $\sim 3.4$  au from the Sun pre-perihelion, and followed it throughout the inner solar system until it reached a heliocentric distance of  $\sim 4$  au post-perihelion. UVOT was able to detect OH for most of the apparition, mea-

asuring water production rates increasing from  $1.8$  to  $20 \times 10^{28}$  molecules/s as the comet approached the Sun (Figure 4). Surprisingly, the water production rates derived from *Swift*/UVOT measurements were initially much larger than those derived from observations with slit-based instruments on Keck, the Very Large Telescope (VLT), and NASA’s Infrared Telescopic Facility (IRTF) [39–41]<sup>1</sup> but in good agreement with large aperture observations using the Solar Wind ANisotropies (SWAN) all-sky hydrogen Lyman-alpha camera on board the Solar and Heliospheric Observatory (SOHO) [42]. Three months after the comet passed the Sun, the production rates measured with these different techniques were all in good agreement. This suggested that, on its approach to the Sun, comet Garradd had an extended source of water in its coma, likely icy grains lifted from the surface that evaporated outside the narrow slits used by spectroscopic instruments on telescopes such as the W. M. Keck Observatory and IRTF. This source of icy grains was depleted during perihelion, after which the production of water vapor was dominated by the nucleus itself [16,42].

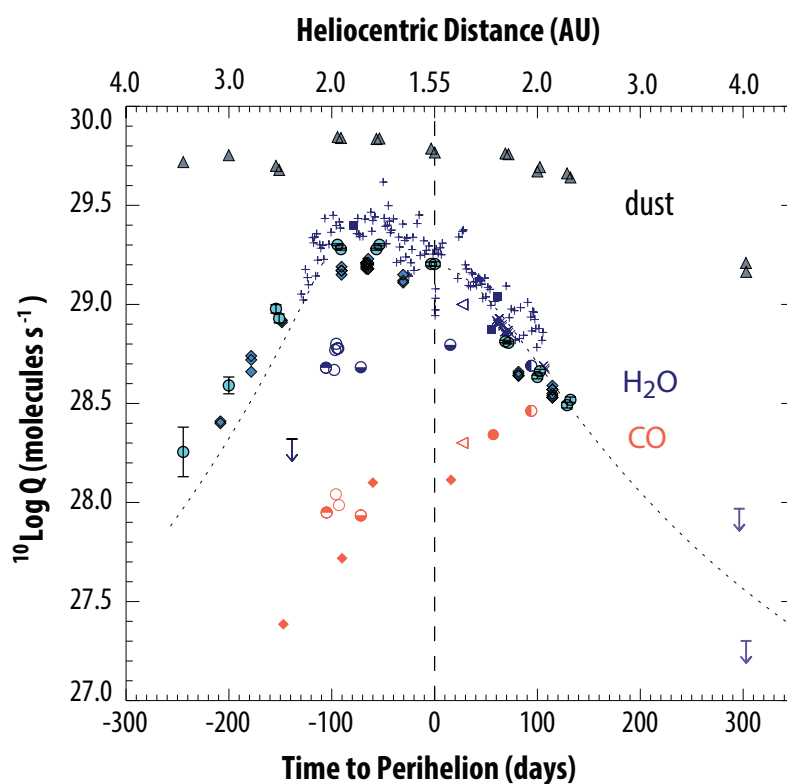


**Figure 4.** Activity evolution of comet C/2009 P1 (Garadd), taken from [16]. H<sub>2</sub>O production rates (blue symbols) peak ~100 days pre-perihelion, while CO (red symbols) continues to increase even after perihelion. Perihelion is indicated by a vertical dashed line. Water production rates derived using imaging with large apertures (*Swift*/UVOT—cyan circles [16]; SOHO/SWAN—blue pluses [42]) are much larger than those derived from observations with slit-based instruments (VLT/CRIRES—blue open circles and downward arrow pre-perihelion—[39]); Keck/NIRSPEC—blue lower half filled circle [40]; Keck/NIRSPEC and IRTF/CSHELL—blue upper half circle [41]). For a complete attribution of all measured production rates, see [16].

A second example of UVOT’s capabilities was its characterization of the water production rates of 2I/Borisov (Figure 5). This object was the second interstellar object discovered passing through our solar system. Borisov displayed clear cometary activity and was available for observations for several months. However, it was a relatively faint object, peaking at a brightness of  $V \sim 17$  [17]. *Swift*/UVOT was uniquely capable of monitoring the object for two months around its perihelion and measured water production between  $5$ – $11 \times 10^{26}$  molecules/s (corresponding to 15–33 kg/s). These values are about an order

of magnitude lower than production rates for typical periodic comets, Borisov was likely a small object with a radius of fewer than 0.5 km [43]. This implied that over 50% of the nucleus surface must have been active during the observation period. The water production rates obtained by *Swift* were essential to the observation that 2I/Borisov was highly enriched in CO compared to regular solar system comets, which may provide clues about its extrasolar origins and its host disk environment [44,45].

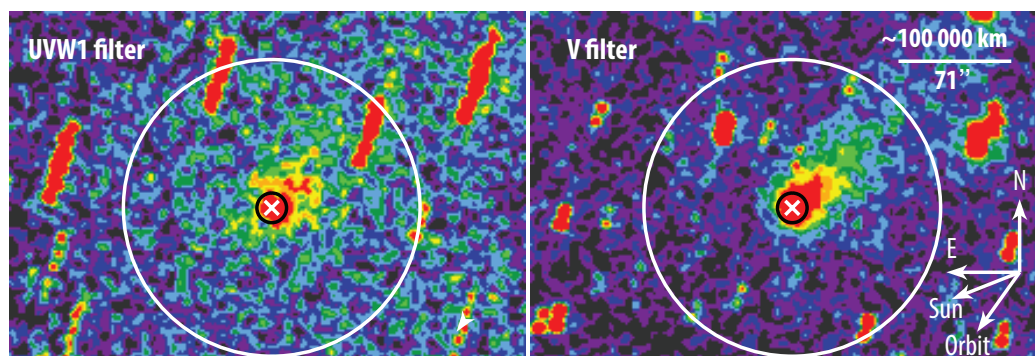


**Figure 5.** UVOT monitored the water production rates of the first active interstellar comet 2I/Borisov throughout the inner solar system by combining UVW1 (left) and V-band filter (right) observations. These observations were acquired on 21 December 2019, when the comet was at 2.03 au from the sun and 1.94 au from Earth, after [17].

### 2.3. Rapid Follow Up on Outburst and Fragmentation Events

Sudden increases in the activity of small bodies indicate disruptive events that may provide insights into physical properties of their nuclei, their volatile content, and their evolution. *Swift*'s rapid follow-up and monitoring capabilities have proven invaluable in the study of such events. In comets, these events can increase an object's brightness by as much as 14.5 mag (17P/Holmes, [46]). Modest (0.1 mag) events may be related to geological events such as cliff collapse (67P/Churyumov–Gerasimenko, [47]), whereas larger events can be related to fragmentation events (73P/Schwassmann–Wachmann 3, [48]) that in some cases are catastrophic (C/1999 S4 (LINEAR) [49]). As described in the Introduction, our current understanding of small bodies suggests that there is a continuum between comets and asteroids [4]. Asteroids can develop a coma and/or dust tail. While repeated activity around perihelion is generally considered evidence of the sublimation of volatiles [50], there are many different processes that can disrupt asteroids and/or release material into space. Those include rotational spin up, leading to fragmentation, electrostatic lofting, thermal fracturing, or impacts [4].

On 11 December 2010, the large, primitive asteroid 596 (Scheila) was discovered to have an unexpected increase in brightness of 1 mag and started developing what appeared to be a coma and tail [51]. This was a very exciting observation, as with the exception of 1 (Ceres), the most known active asteroids were relatively small objects with diameters of up to 5 km, whereas Scheila has a diameter of 160 km [4]. *Swift* observed the asteroid within days of the first announcement of the activity and acquired imaging and grism spectroscopy to investigate what caused this activity [6]. The UVOT images revealed two large ejecta clouds (Figure 6). Both the UVW1–V photometric colors of the dust and grism spectra ruled out the presence of significant amounts of OH, and thus H<sub>2</sub>O. In addition, the plumes faded rapidly [52]. These observations ruled out the sublimation of water ice as the driver of activity. Instead, the plumes were caused by the impact of a much smaller asteroid (30–80 m in diameter, [6,52–54]). As such, Scheila was the first time the immediate aftermath of the collision between two asteroids was observed, allowing us to study a sub-critical impact on a primitive asteroid. Such an impact will have created a crater of about a kilometer in diameter, but subsequent observations of Scheila's lightcurve imply that a much larger area on its surface was altered by the impact [55].

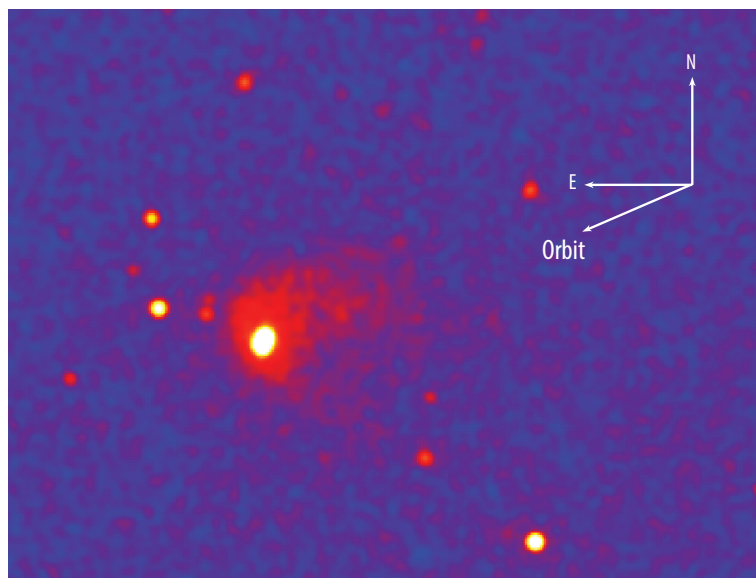


**Figure 6.** UVOT V-band imaging of the aftermath of the impact on asteroid 596 (Scheila). Two plumes are visible, containing a total of  $6 \times 10^8$  kg of ejected dust. UVOT grism spectroscopy ruled out that the plumes contained water vapor, implying that the activity was triggered by a collision with a small asteroid [6]. The asteroid's orbital direction and the direction to the Sun are approximately aligned.

#### 2.4. Ultraviolet Spectroscopy of Asteroids

Reflectance spectra of airless small bodies in the solar system allow for the remote characterization of their surface properties. Traditionally, visible, near-infrared spectroscopic data have been used to study the surface composition of solar system bodies and to connect them to meteoritic samples [56,57]. Laboratory measurements, space missions, and remote observations demonstrate that asteroidal UV spectra can be more sensitive to mineral properties and space weathering effects than the reflectance spectra at longer wavelengths [58–60]. However, only the dataset acquired by the International Ultraviolet Explorer (IUE, [61–63]) from more than a decade ago and a few scattered observations exist in the UV (c.f., [60,64–67]). In addition, the instrumental noise of IUE renders the spectra only reliable between 2400–3200 Å, leaving an observational gap between the near-UV waveband and ground-based surveys such as the Small Main-Belt Asteroid Spectroscopic Survey (SMASS [68,69]).

To expand the dataset of asteroidal reflectance spectra observed in the near ultraviolet, *Swift*/UVOT conducted a systematic survey of 18 asteroids of distinct spectral types using the UV grism. However, *Swift* did not track the asteroids and the spectral extraction of grism observations of small bodies is not trivial, albeit less elaborate than those of comets [70], because the asteroids can be treated as smeared point sources. To extract asteroidal spectra from grism images, we use the UVOTPY procedure outlined in Kuin et al. [14], with some modifications required for our science case. Grism images can be contaminated by background stars, and we combine grism images of the target to remove those. Next, we determine the anchor position of the asteroid in the grism image using its ephemerides from JPL/Horizons<sup>2</sup>. This also allows us to evaluate the relative motion of the asteroid due to its apparent motion during the exposure and hence the optimal extraction width of the spectrum. The spectrum can then be extracted and straightened. The flux and wavelength are performed as outlined in Kuin et al. [14], with corrections made for the aperture size, sensitivity decrease, and co-incidence loss (see also Section 1). To calculate the reflectance, the extracted spectrum is divided by that of a solar analog, GSPC P41-C or GSPC P177-D, which were both observed with UVOT's UV grism as well as the Space Telescope Imaging Spectrograph (STIS) on the Hubble Space Telescope (HST; [71]).

An example reflectance spectrum of (3) Juno is shown in Figure 7. Juno was observed on 20 April 2011, at a distance of 2.9 au from the Sun and 2.1 au from Earth. At the time

of the observations, it has a visible magnitude  $m_V \approx 9.7$ , as such avoiding significant coincidence loss at the visible end of the spectrum while providing good signal-to-noise ratios in the UV part. The results are in excellent agreement with archival observations of IUE, MMT, and SMASS surveys, demonstrating that UVOT is uniquely suited to connect those data and thus fill in critical data gaps of asteroid reflectance spectra.

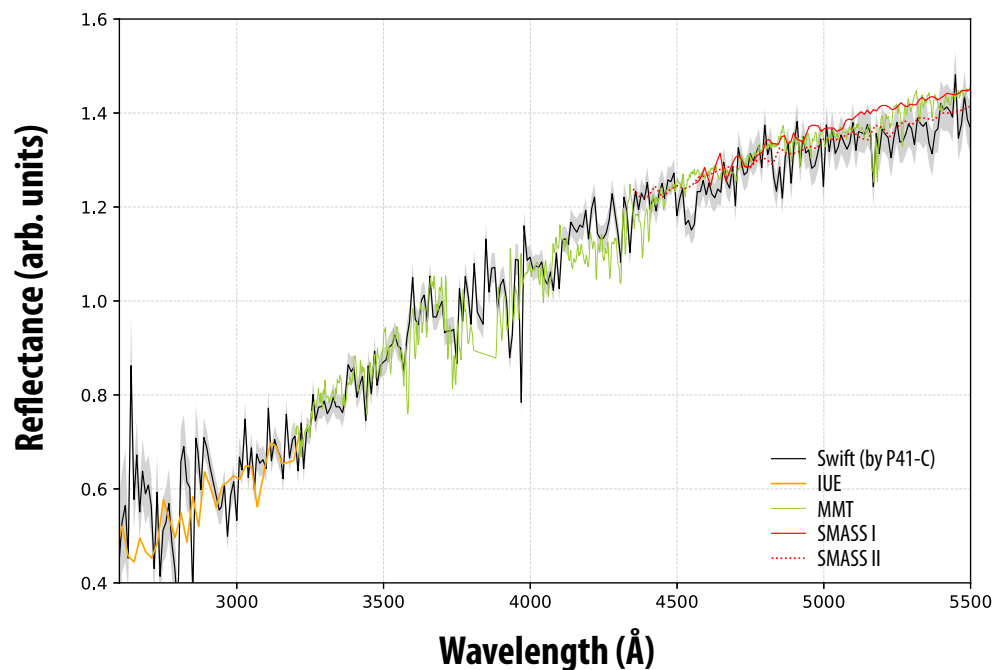


**Figure 7.** Reflectance spectra of asteroid (3) Juno. The black curve is the reflectance spectrum observed by *Swift*/UVOT, normalized around 3800 Å. The shaded area around the spectrum marks the  $1\text{-}\sigma$  uncertainties. The orange curve is the IUE reflectance spectrum [63], which is scaled to more clearly compare with the UVOT spectrum. The green curve is the scaled reflectance spectrum measured with the MMT 6m telescope [60]. The scaled red solid curve and the scaled red dotted curve were respectively measured by SMASS I [68] and SMASS II surveys [69].

### 2.5. Grism Spectroscopy of Comets

Grism spectroscopy is well-suited for observing extended objects, as it combines high sensitivity with spatially resolved spectroscopy over large extended areas. Grism images of extended objects are two-dimensional; on the dispersion axis, the spatial distribution of gas and dust in the coma are convolved, but the direction perpendicular to the dispersion axis depends purely on the morphology of the emission mapped (Figure 8).

To preserve the spatial information, rather than extracting and reducing the spectrum as was described for UVOT asteroid observations with the gratings (Section 2.5), a method commonly used to analyze grism images of comets is forward modeling [70,72]. For near UV and optical wavelengths, this is feasible because the spectrum and spatial distribution of the relevant species is reasonably well known (c.f., [36,73,74]), and, at the low resolution, it is dominated by a limited number of spectral features. The methodology for the analysis of UVOT grism observations of comets was laid out in Bodewits et al. [70]. In brief, background stars and their spectra are removed by comparing subsequent exposures of the comet, which will move with respect to these stars. Individual exposures are then stacked to increase the signal-to-noise ratio and rotated so that the dispersion axis of the first order is aligned horizontally (Figure 8). A major difference with the asteroid grism observations is that, for comets, the 0th order image of the comet is an extended background source that fills most if not the entire image. As such, it also contributed significantly to coincidence loss in the regions of interest, an issue that is yet to be addressed. The 0th order is effectively a broad band image of the comet and is mostly dominated by continuum emission from



sunlight reflected by dust (Figure 1). It can be effectively removed by subtracting a median radial surface brightness profile. The resulting clean image resembles ‘pearls on a string’. The dust in the coma has a more condensed distribution, and the continuum is therefore a spatially narrower feature than the gas, which typically spans hundreds of thousands of kilometers for fragment species seen in the near UV/optical wavelengths (Figure 2).

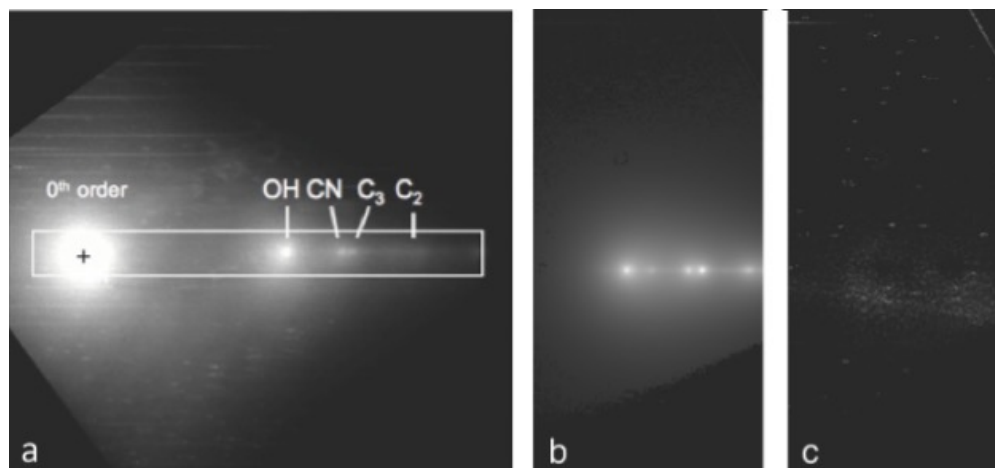


**Figure 8.** UVOT Grism spectroscopy combined with forward modeling allows us to reliably measure production rates and abundances with *Swift*/UVOT. (a) observed, stacked grism image of comet C/2007 N3 (Lulin); (b) modeled grism image; (c) residual image where the 2D model image is subtracted from the observed grism image, adapted from Bodewits et al. [70].

To model the grism image and derive column densities of the fragment species of interest, we create radial profiles of each of the expected emission in a particular line or spectroscopically unresolved band. We offset the resulting coma image according to the grism dispersion relation from the astrometric center of the comet. Next, we convolve the image by an estimate of the point spread function in grism mode, which we create by making a figure from the cross-dispersion profile model generated from stellar spectra in the grism-mode image by the pipeline processing system. We then sum the results and arrive at the best-fit set of parameters by minimizing the  $\chi^2$  of the residual between the model and data images and adjusting the parameters using a parameter optimizer.

It is the combination of spectral/spatial vs. spatial axis that allows for unique model solutions to the grism images, even when the specific scale length of a gas is unknown. We demonstrated in Bodewits et al. [70] that the forward modeling technique successfully extracted production rates for OH, CS, NH, CN, C<sub>3</sub>, and C<sub>2</sub> for comet C/2007 N3 (Lulin). Forward modeling techniques are highly sensitive because of the large number of pixels that ultimately participate in the  $\chi^2$  minimization process. This is the advantage of using a 2D imaging technique where the field of view of the image is large enough to encompass a significant amount of the coma emissions being studied. Forward modeling of grism spectra is therefore a reliable method for deriving gas and dust production rates.

### 2.6. Contemporaneous X-ray and UV Observations

*Swift* typically operates all its instruments simultaneously. Whereas UVOT has been the main science driver for most of *Swift*'s small body observations, the combined observations in the X-ray and UV domains have proven valuable in several comet observations [37,75,76]. Comets can emit up to around 1 GW in soft X-rays, mostly at photon energies below 1 keV, through charge exchange between highly charged solar wind ions with neutral molecules in the coma [77,78]. Since the initial discovery of charge exchange emission from comet C/1996 B2 (Hyakutake) [79], many comets have been observed in X-rays (c.f., [80,81]). X-rays provide a unique window on physical processes in the coma, such as the velocity and ionization state of the local solar wind interacting with

the comet [80,82–84], the location of plasma boundaries [85], the distribution [86,87], and likely even the chemical composition of the neutral gas [74,88].

Whereas *Swift* observed dozens of comets, its X-ray Telescope (XRT) has an effective area of 5–100 cm<sup>2</sup> between photon energies of 200–1000 eV [89], implying that it can only detect very bright comets. As of the current date, there are three *Swift* observing campaigns that reported combined UV and X-ray observations. The first was a monitoring campaign centered around the *Deep Impact* mission to comet 9P/Tempel 1 [90]. *Swift* started observing the comets about 2 weeks before until 65 days after the man-made impactor hit its nucleus. The *Swift* observations resulted in two separate papers [75,91], both discussing the mass of volatiles excavated by the event, one of the main parameters that were to be determined remotely following the impact experiment [92]. Both UVOT and XRT are well-suited to address these questions. As discussed in Section 2.2, UVOT's UVW1 filter includes the emission of the OH radical and thus traces water. The UVOT results suggested that  $4.2 \times 10^6$  kg of water was released [91]. The X-ray intensity traces the solar wind variability and the amount of neutral gas available and is therefore agnostic of the type of gas released. Comparing the enhanced X-ray brightness with the comet's baseline brightness, Willingale et al. [75] derived that the impact released  $2 \times 10^8$  kg of water ice. The UVOT results are in line with other observing campaigns that reported masses for the water ice ( $4\text{--}9 \times 10^6$  kg, [92]), adding that other volatiles could add tens of percent at most. The divergence between the XRT and UVOT results might be attributed to short-term variations in the solar wind [76,93] and certainly warrants further investigation.

The apparition of comet C/2007 N3 (Lulin) offered a bright comet ( $m_V \sim 7$ ) that allowed for the first simultaneous imaging of a comet in X-ray and UV wavelengths (Figure 9 [37,70]). These observations for the first time allowed the direct comparison of the distribution of the gaseous coma (OH, in the case of UVOT) with the plasma interaction with the solar wind. At water production rates of  $5 \times 10^{28}$  molecules/s, the comet was moderately collisionally thick to charge exchange [80], resulting in an X-ray stand-off distance of 35,000 km at the comet (not corrected for geometrical projection). A similar campaign was pursued for the very close approach of comet 46P/Wirtanen, which reached within 0.0775 au ( $11.5 \times 10^6$  km) of Earth in December 2018. *Swift* observed it three times between 28 November 2018 and 12 January 2019, and it reached  $m_V \sim 7$  during the 13 December observations. This was comparable to the total brightness of comet Lulin, which had a gas production rate that was five times higher than Wirtanen, but which was 6.5 times further away from Earth during its *Swift* observations. At 5.0 MW, the X-ray luminosity of 46P turned out to be the lowest ever detected for a comet—owing to a combination of the comet's low gas production rate ( $1 \times 10^{28}$  molecules/s) and the low ionization state and ion flux of the solar wind during the observations [76]. *Swift's* combined X-ray and UV observations clearly illustrate that a comet's X-ray luminosity is primarily driven and modulated by the solar wind that it can therefore vary on timescales as short as hours, and that the brightness of a comet at visible wavelengths (mostly governed by its dust content) is not a direct predictor of its X-ray luminosity (driven by solar wind conditions and the comet's gas content). The Wirtanen campaign emphasized that cometary X-ray campaigns provide the opportunity to remotely sample comet-solar wind plasma interactions for a range of conditions within a single observing campaign.

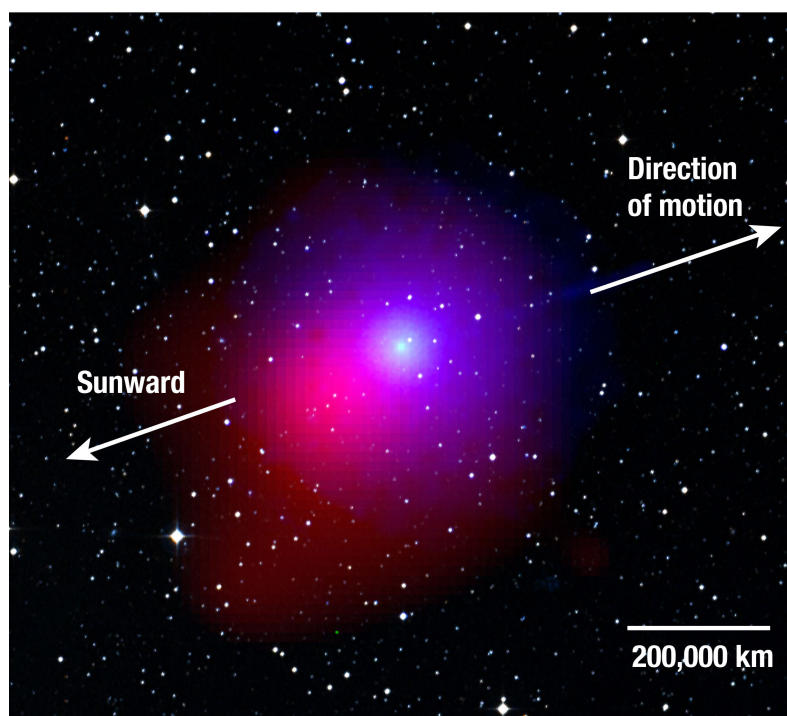


**Figure 9.** Combined *Swift*-UVOT and X-ray Telescope observations of comet C/2007 N3 (Lulin). This bright comet allowed UVOT to image the cloud of OH radicals in its coma (blue) and XRT to detect X-rays produced by solar wind charge exchange (red). Because of the comet's large gas production rates, the coma is collisionally thick to charge exchange and is thus offset towards the direction of the Sun (after [37,74]).

### 3. Conclusions

Data from the *Neil Gehrels–Swift Observatory* have greatly extended our understanding of the solar system. Its combination of multi-wavelength coverage, rapid response, and monitoring capabilities have proven to be very valuable in the study of small bodies. Many properties of comets and asteroids are revealed through their variability over time, which can be related to their illumination and heating, such as diurnal, seasonal, and orbital activity variation. Sudden, short-lived events such as outbursts, fragmentation, and impact events can uncover physical and chemical information about the objects otherwise not accessible. Furthermore, the ultraviolet wavelengths encompassed by UVOT cover features that directly trace the sublimation of water (through OH) and the signatures of space weathering in asteroids. As such, *Swift* has proven to be invaluable in the study of the properties and evolution of small bodies in our solar system.

**Author Contributions:** All authors contributed to writing, editing, and reviewing. All authors have read and agreed to the published version of the manuscript.

**Funding:** We gratefully acknowledge support from the Neil Gehrels–Swift Observatory Guest Observer program, as well as support through NASA's Planetary Data Archiving, Restoration and Tools program (NNX17AK99G-PI Morgenthaler, and NNX17AL24G-PI Hendrix).

**Data Availability Statement:** The data underlying this paper are available in the *Swift* archive at [https://www.swift.ac.uk/swift\\_live/](https://www.swift.ac.uk/swift_live/) and the HEASARC Browse archive at <https://heasarc.gsfc.nasa.gov/cgi-bin/W3Browse/w3browse.pl> (accessed on 1 December 2022).

**Acknowledgments:** This work represents the efforts of many collaborators, principally Jenny Carter, Stefan Immler, Geronimo Villanueva, Paul Kuin, Wayne Landsman, Sam Oates, Tony Farnham, Mike Kelley, Jian Yang Li, Andy Read, Amanda Hendrix, Faith Vilas, and Emanuele Bonamente. We thank the *Swift* team, in particular Neil Gehrels, Brad Cenko, Mike Siegel, Jeff Gropp, Boris Sbarufatti, Tineke Roegiers, and Margaret Chester for their efforts in facilitating, planning, and executing these difficult observations.

**Conflicts of Interest:** The authors declare no conflict of interest.

## Notes

- <sup>1</sup> for example, observations with CSHELL at NASA-IRTF use a typical slit size of  $1.0 \times 30$  arcsec, whereas UVOT's FOV is  $17 \text{ arcmin} \times 17 \text{ arcmin}$ .
- <sup>2</sup> <https://ssd.jpl.nasa.gov/horizons/>, accessed on 1 December 2022.

## References

- Rubin, M.; Bekaert, D.V.; Broadley, M.W.; Drozdovskaya, M.N.; Wampfler, S.F. Volatile Species in Comet 67P/Churyumov-Gerasimenko: Investigating the Link from the ISM to the Terrestrial Planets. *ACS Earth Space Chem.* **2019**, *3*, 1792–1811.
- Altwegg, K.; Team, R. Chemical highlights from the Rosetta mission. *Astrochem. VII Through Cosm. Galaxies Planets* **2018**, *332*, 153–162. [[CrossRef](#)]
- McKay, A.; Roth, N. Organic Matter in Cometary Environments. *Life* **2021**, *11*, 37. [[CrossRef](#)] [[PubMed](#)]
- Jewitt, D.; Hsieh, H.H. The Asteroid-Comet Continuum. *arXiv* **2022**, arXiv:2203.01397.
- Snodgrass, C.; Tubiana, C.; Vincent, J.B.; Sierks, H.; Hviid, S.F.; Moissi, R.; Boehnhardt, H.; Barbieri, C.; Koschny, D.; Lamy, P.L.; et al. A collision in 2009 as the origin of the debris trail of asteroid P/2010A2. *Nature* **2010**, *467*, 814. [[CrossRef](#)]
- Bodewits, D.; Kelley, M.S.; Li, J.Y.; Landsman, W.B.; Besse, S.; A'Hearn, M.F. Collisional Excavation of Asteroid (596) Scheila. *Astrophys. J. Lett.* **2011**, *733*, L3. [[CrossRef](#)]
- Choukroun, M.; Altwegg, K.; Kühr, E.; Biver, N.; Bockelée-Morvan, D.; Drażkowska, J.; Hérique, A.; Hilchenbach, M.; Marschall, R.; Pätzold, M.; et al. Dust-to-Gas and Refractory-to-Ice Mass Ratios of Comet 67P/Churyumov-Gerasimenko from Rosetta Observations. *Space Sci. Rev.* **2020**, *216*, 44. [[CrossRef](#)]
- Hahn, G.; Rickman, H. Asteroids in cometary orbits. *Icarus* **1985**, *61*, 417–442. [[CrossRef](#)]
- Meech, K.J.; Yang, B.; Kleyna, J.; Hainaut, O.R.; Berdyugina, S.; Keane, J.V.; Micheli, M.; Morbidelli, A.; Wainscoat, R.J. Inner solar system material discovered in the Oort cloud. *Sci. Adv.* **2016**, *2*, e1600038. [[CrossRef](#)]
- Gehrels, N.; Chincarini, G.; Giommi, P.; Mason, K.O.; Nousek, J.A.; Wells, A.A.; White, N.E.; Barthelmy, S.D.; Burrows, D.N.; Cominsky, L.R.; et al. The Swift Gamma-Ray Burst Mission. *Astrophys. J.* **2004**, *611*, 1005–1020.
- Roming, P.W.A.; Kennedy, T.E.; Mason, K.O.; Nousek, J.A.; Ahr, L.; Bingham, R.E.; Broos, P.S.; Carter, M.J.; Hancock, B.K.; Huckle, H.E.; et al. The Swift Ultra-Violet/Optical Telescope. *Space Sci. Rev.* **2005**, *120*, 95–142.
- Mason, K.O.; Breeveld, A.; Hunsberger, S.D.; James, C.; Kennedy, T.E.; Roming, P.W.A.; Stock, J. Performance of the UV/Optical Telescope (UVOT) on SWIFT. *X-ray Gamma-Ray Instrum. Astron. XIII* **2004**, *5165*, 277–286. [[CrossRef](#)]
- Breeveld, A.A.; Curran, P.A.; Hoversten, E.A.; Koch, S.; Landsman, W.B.; Marshall, F.E.; Page, M.J.; Poole, T.S.; Roming, P.W.A.; Smith, P.J.; et al. Further calibration of the Swift ultraviolet/optical telescope. *Mon. Not. R. Astron. Soc.* **2010**, *406*, 1687–1700. [[CrossRef](#)]
- Kuin, N.P.M.; Landsman, W.B.; Breeveld, A.A.; Page, M.J.; Lamoureux, H.; James, C.; Mehdipour, M.; Still, M.; Yershov, V.; Brown, P.J.; et al. Calibration of the Swift-UVOT ultraviolet and visible grisms. *Mon. Not. R. Astron. Soc.* **2015**, *449*, 2514–2538. [[CrossRef](#)]
- Fordham, J.L.A.; Moorhead, C.F.; Galbraith, R.F. Dynamic-range limitations of intensified CCD photon-counting detectors. *Mon. Not. R. Astron. Soc.* **2000**, *312*, 83–88. [[CrossRef](#)]
- Bodewits, D.; Farnham, T.L.; A'Hearn, M.F.; Feaga, L.M.; McKay, A.J.; Schleicher, D.G.; Sunshine, J.M. The Evolving Activity of the Dynamically Young Comet C/2009 P1 (Garradd). *Astrophys. J.* **2014**, *786*, 48. [[CrossRef](#)]
- Xing, Z.; Bodewits, D.; Noonan, J.; Bannister, M.T. Water Production Rates and Activity of Interstellar Comet 2I/Borisov. *Astrophys. J. Lett.* **2020**, *893*, L48.
- Villanueva, G.L.; Smith, M.D.; Protopapa, S.; Faggi, S.; Mandell, A.M. Planetary Spectrum Generator: An accurate online radiative transfer suite for atmospheres, comets, small bodies and exoplanets. *J. Quant. Spectrosc. Radiat. Transf.* **2018**, *217*, 86–104.
- Combi, M.R.; Mäkinen, T.; Bertaux, J.L.; Quémerais, E.; Ferron, S.; Coronel, R. Comet 41P/Tuttle–Giacobini–Kresak, 45P/Honda–Mrkos–Pajdusakova, and 46P/Wirtanen: Water Production Activity over 21 yr with SOHO/SWAN. *Planet. Sci. J.* **2020**, *1*, 72. [[CrossRef](#)]
- Bodewits, D.; Farnham, T.L.; Kelley, M.S.; Knight, M.M. A rapid decrease in the rotation rate of comet 41P/Tuttle–Giacobini–Kresak. *Nature* **2018**, *553*, 186–188. [[CrossRef](#)]
- Schleicher, D.G.; Knight, M.M.; Eisner, N.L.; Thirouin, A. Gas Jet Morphology and the Very Rapidly Increasing Rotation Period of Comet 41P/Tuttle–Giacobini–Kresak. *Astron. J.* **2019**, *157*, 108.
- Moulane, Y.; Jehin, E.; Opitom, C.; Pozuelos, F.J.; Manfroid, J.; Benkhaldoun, Z.; Daassou, A.; Gillon, M. Monitoring of the activity and composition of comets 41P/Tuttle–Giacobini–Kresak and 45P/Honda–Mrkos–Pajdusakova. *Astron. Astrophys.* **2018**, *619*, A156.
- Farnham, T.L.; Kelley, M.S.P.; Bodewits, D.; Knight, M.M.; Thirouin, A.; Moskovitz, N. *Comet 41P/Tuttle–Giacobini–Kresak*; CBET: San Antonio, TX, USA, 2017; Volume 4375.
- Keller, H.U.; Mottola, S.; Skorov, Y.; Jorda, L. The changing rotation period of comet 67P/Churyumov-Gerasimenko controlled by its activity. *Astron. Astrophys.* **2015**, *579*, L5. [[CrossRef](#)]

25. Gutiérrez, P.J.; Jorda, L.; Gaskell, R.W.; Davidsson, B.J.R.; Capanna, C.; Hviid, S.F.; Keller, H.U.; Maquet, L.; Mottola, S.; Preusker, F.; et al. Possible interpretation of the precession of comet 67P/Churyumov-Gerasimenko. *Astron. Astrophys.* **2016**, *590*, A46. [[CrossRef](#)]
26. Gutiérrez, P.J.; Jorda, L.; Ortiz, J.L.; Rodrigo, R. Long-term simulations of the rotational state of small irregular cometary nuclei. *Astron. Astrophys.* **2003**, *406*, 1123–1133. [[CrossRef](#)]
27. Knight, M.M.; Eisner, N.; Schleicher, D.G.; Thirouin, A. *Comet 41P/Tuttle–Giacobini–Kresák*; CBET: San Antonio, TX, USA, 2017; Volume 4377.
28. Keller, H.U.; Kühr, E. Cometary Nuclei—From Giotto to Rosetta. *Space Sci. Rev.* **2020**, *216*, 14–26. [[CrossRef](#)]
29. A’Hearn, M.F. Comets: Looking ahead. *Philos. Trans. R. Soc. Lond. Ser. A* **2017**, *375*, 20160261. [[CrossRef](#)]
30. Ciarniello, M.; Fulle, M.; Raponi, A.; Filacchione, G.; Capaccioni, F.; Rotundi, A.; Rinaldi, G.; Formisano, M.; Magni, G.; Tosi, F.; et al. Macro and micro structures of pebble-made cometary nuclei reconciled by seasonal evolution. *Nat. Astron.* **2022**, *6*, 546–553. [[CrossRef](#)]
31. Protopapa, S.; Kelley, M.S.P.; Yang, B.; Bauer, J.M.; Kolokolova, L.; Woodward, C.E.; Keane, J.V.; Sunshine, J.M. Icy Grains from the Nucleus of Comet C/2013 US10 (Catalina). *Astrophys. J. Lett.* **2018**, *862*, L16,
32. A’Hearn, M.F.; Belton, M.J.S.; Delamere, W.A.; Feaga, L.M.; Hampton, D.; Kissel, J.; Klaasen, K.P.; McFadden, L.A.; Meech, K.J.; Melosh, H.J.; et al. EPOXI at Comet Hartley 2. *Science* **2011**, *332*, 1396–1400. [[CrossRef](#)]
33. Bonev, B.P.; Dello Russo, N.; DiSanti, M.A.; Martin, E.C.; Doppmann, G.; Vervack Ronald, J.J.; Villanueva, G.L.; Kawakita, H.; Gibb, E.L.; Combi, M.R.; et al. First Comet Observations with NIRSPEC-2 at Keck: Outgassing Sources of Parent Volatiles and Abundances Based on Alternative Taxonomic Compositional Baselines in 46P/Wirtanen. *Planet. Sci. J.* **2021**, *2*, 45. [[CrossRef](#)]
34. Capria, M.T.; Capaccioni, F.; Filacchione, G.; Tosi, F.; De Sanctis, M.C.; Mottola, S.; Ciarniello, M.; Formisano, M.; Longobardo, A.; Migliorini, A.; et al. How pristine is the interior of the comet 67P/Churyumov-Gerasimenko? *Mon. Not. R. Astron. Soc.* **2017**, *469*, S685–S694. [[CrossRef](#)]
35. Biver, N.; Dello Russo, N.; Opitom, C.; Rubin, M. Chemistry of comet atmospheres. *arXiv* **2022**, arXiv:2207.04800.
36. A’Hearn, M.F.; Millis, R.L.; Schleicher, D.G.; Osip, D.J.; Birch, P.V. The ensemble properties of comets: Results from narrowband photometry of 85 comets, 1976–1992. *Icarus* **1995**, *118*, 223. [[CrossRef](#)]
37. Carter, J.A.; Bodewits, D.; Read, A.M.; Immler, S.M. Simultaneous Swift X-ray and UV views of comet C/2007 N3 (Lulin). *Astron. Astrophys.* **2012**, *541*, 70. [[CrossRef](#)]
38. Farnham, T.L.; Schleicher, D.G.; A’Hearn, M.F. The HB Narrowband Comet Filters: Standard Stars and Calibrations. *Icarus* **2000**, *147*, 180. [[CrossRef](#)]
39. Paganini, L.; Mumma, M.J.; Villanueva, G.L.; DiSanti, M.A.; Bonev, B.P.; Lippi, M.; Boehnhardt, H. The Chemical Composition of CO-rich Comet C/2009 P1 (Garradd) AT  $R_h = 2.4$  and 2.0 AU before Perihelion. *Astrophys. J. Lett.* **2012**, *748*, L13,
40. DiSanti, M.A.; Villanueva, G.L.; Paganini, L.; Bonev, B.P.; Keane, J.V.; Meech, K.J.; Mumma, M.J. Pre- and post-perihelion observations of C/2009 P1 (Garradd): Evidence for an oxygen-rich heritage? *Icarus* **2014**, *228*, 167–180. [[CrossRef](#)]
41. Villanueva, G.L.; Mumma, M.J.; DiSanti, M.A.; Bonev, B.P.; Paganini, L.; Blake, G.A. A multi-instrument study of Comet C/2009 P1 (Garradd) at 2.1 AU (pre-perihelion) from the Sun. *Icarus* **2012**, *220*, 291–295. [[CrossRef](#)]
42. Combi, M.R.; Mäkinen, J.T.T.; Bertaux, J.L.; Quémerais, E.; Ferron, S.; Fougere, N. Water production rate of Comet C/2009 P1 (Garradd) throughout the 2011–2012 apparition: Evidence for an icy grain halo. *Icarus* **2013**, *225*, 740–748. [[CrossRef](#)]
43. Jewitt, D.; Luu, J. Initial Characterization of Interstellar Comet 2I/2019 Q4 (Borisov). *Astrophys. J. Lett.* **2019**, *886*, L29,
44. Bodewits, D.; Noonan, J.W.; Feldman, P.D.; Bannister, M.T.; Farnocchia, D.; Harris, W.M.; Li, J.Y.; Mandt, K.E.; Parker, J.W.; Xing, Z.X. The carbon monoxide-rich interstellar comet 2I/Borisov. *Nat. Astron.* **2020**, *4*, 867–871.
45. Cordiner, M.A.; Milam, S.N.; Biver, N.; Bockelee-Morvan, D.; Roth, N.X.; Bergin, E.A.; Jehin, E.; Remijan, A.J.; Charnley, S.B.; Mumma, M.J.; et al. Unusually high CO abundance of the first active interstellar comet. *Nat. Astron.* **2020**, 1–6. [[CrossRef](#)]
46. Lin, Z.Y.; Lin, C.S.; Ip, W.H.; Lara, L.M. The Outburst of Comet 17p/Holmes. *Astron. J.* **2009**, *138*, 625–632. [[CrossRef](#)]
47. Pajola, M.; Höfner, S.; Vincent, J.B.; Oklay, N.; Scholten, F.; Preusker, F.; Mottola, S.; Naletto, G.; Fornasier, S.; Lowry, S.; et al. The pristine interior of comet 67P revealed by the combined Aswan outburst and cliff collapse. *Nat. Astron.* **2017**, *1*, 0092. [[CrossRef](#)]
48. Reach, W.T.; Vaubaillon, J.; Kelley, M.S.; Lisse, C.M.; Sykes, M.V. Distribution and properties of fragments and debris from the split Comet 73P/Schwassmann-Wachmann 3 as revealed by Spitzer Space Telescope. *Icarus* **2009**, *203*, 571–588.
49. Farnham, T.L.; Schleicher, D.G.; Woodney, L.M.; Birch, P.V.; Eberhardy, C.A.; Levy, L. Imaging and Photometry of Comet C/1999 S4 (LINEAR) Before Perihelion and After Breakup. *Science* **2001**, *292*, 1348–1353. [[CrossRef](#)]
50. Hsieh, H.H.; Jewitt, D. A Population of Comets in the Main Asteroid Belt. *Science* **2006**, *312*, 561–563. [[CrossRef](#)]
51. Larson, S.M. (596) Scheila. *IAU Circ.* **2010**, *9188*, 1.
52. Jewitt, D.; Weaver, H.A.; Mutchler, M.J.; Larson, S.M.; Agarwal, J. Hubble Space Telescope Observations of Main-belt Comet (596) Scheila. *Astrophys. J. Lett.* **2011**, *733*, L4. [[CrossRef](#)]
53. Ishiguro, M.; Hanayama, H.; Hasegawa, S.; Sarugaku, Y.; Watanabe, J.i.; Fujiwara, H.; Terada, H.; Hsieh, H.H.; Vaubaillon, J.J.; Kawai, N.; et al. Interpretation of (596) Scheila’s Triple Dust Tails. *Astrophys. J. Lett.* **2011**, *741*, L24,
54. Moreno, F.; Licandro, J.; Ortiz, J.L.; Lara, L.M.; Alí-Lagoa, V.; Vaduvescu, O.; Morales, N.; Molina, A.; Lin, Z.Y. (596) Scheila in Outburst: A Probable Collision Event in the Main Asteroid Belt. *Astrophys. J.* **2011**, *738*, 130. [[CrossRef](#)]
55. Bodewits, D.; Vincent, J.B.; Kelley, M.S. Scheila’s scar: Direct evidence of impact surface alteration on a primitive asteroid. *Icarus* **2014**, *229*, 190–195. [[CrossRef](#)]

56. Gaffey, M.J. Space weathering and the interpretation of asteroid reflectance spectra. *Icarus* **2010**, *209*, 564–574. [[CrossRef](#)]
57. Clark, B.E.; Binzel, R.P.; Howell, E.S.; Cloutis, E.A.; Ockert-Bell, M.; Christensen, P.; Barucci, M.A.; DeMeo, F.; Lauretta, D.S.; Connolly, H.; et al. Asteroid (101955) 1999 RQ36: Spectroscopy from 0.4 to 2.4  $\mu\text{m}$  and meteorite analogs. *Icarus* **2011**, *216*, 462–475. [[CrossRef](#)]
58. Cloutis, E.A.; McCormack, K.A.; Bell, J.F.; Hendrix, A.R.; Bailey, D.T.; Craig, M.A.; Mertzman, S.A.; Robinson, M.S.; Riner, M.A. Ultraviolet spectral reflectance properties of common planetary minerals. *Icarus* **2008**, *197*, 321–347. [[CrossRef](#)]
59. Hendrix, A.R.; Vilas, F. C-Complex Asteroids: UV-Visible Spectral Characteristics and Implications for Space Weathering Effects. *Geophys. Res. Lett.* **2019**, *46*, 14307–14317. [[CrossRef](#)]
60. Vilas, F.; Hendrix, A.R. The UV/Blue Effects of Space Weathering Manifested in S-Complex Asteroids. I. Quantifying Change with Asteroid Age. *Astron. J.* **2015**, *150*, 64. [[CrossRef](#)]
61. Butterworth, P.S.; Meadows, A.J.; Hunt, G.E.; Moore, V.; Willis, D.M. Ultraviolet spectra of asteroids. *Nature* **1980**, *287*, 701–703. [[CrossRef](#)]
62. Butterworth, P.; Meadows, A. Ultraviolet reflectance properties of asteroids. *Icarus* **1985**, *62*, 305–318. [[CrossRef](#)]
63. Roettger, E.E.; Buratti, B.J. Ultraviolet Spectra and Geometric Albedos of 45 Asteroids. *Icarus* **1994**, *112*, 496–512. [[CrossRef](#)]
64. A'Hearn, M.F.; Feaga, L.M.; Bertaux, J.L.; Feldman, P.D.; Parker, J.W.; Slater, D.C.; Steffl, A.J.; Alan Stern, S.; Throop, H.; Versteeg, M.; et al. The far-ultraviolet albedo of Steins measured with Rosetta-ALICE. *Planet. Space Sci.* **2010**, *58*, 1088–1096. [[CrossRef](#)]
65. Stern, S.A.; Parker, J.W.; Feldman, P.D.; Weaver, H.A.; Steffl, A.; A'Hearn, M.F.; Feaga, L.; Birath, E.; Graps, A.; Bertaux, J.L.; et al. Ultraviolet discoveries at asteroid (21) lutetia by the rosetta alice ultraviolet spectrograph. *Astron. J.* **2011**, *141*, 199. [[CrossRef](#)]
66. Li, J.Y.; Bodewits, D.; Feaga, L.M.; Landsman, W.; A'Hearn, M.F.; Mutchler, M.J.; Russell, C.T.; McFadden, L.A.; Raymond, C.A. Ultraviolet spectroscopy of Asteroid (4) Vesta. *Icarus* **2011**, *216*, 640–649.
67. Becker, T.M.; Cunningham, N.; Molyneux, P.; Roth, L.; Feaga, L.M.; Retherford, K.D.; Landsman, Z.A.; Peavler, E.; Elkins-Tanton, L.T.; Walhund, J.E. HST UV Observations of Asteroid (16) Psyche. *Planet. Sci. J.* **2020**, *1*, 53. [[CrossRef](#)]
68. Xu, S.; Binzel, R.P.; Burbine, T.H.; Bus, S.J. Small Main-belt Asteroid Spectroscopic Survey: Initial results. *Icarus* **1995**, *115*, 1–35. [[CrossRef](#)]
69. Bus, S.J.; Binzel, R.P. Phase II of the Small Main-Belt Asteroid Spectroscopic Survey. A Feature-Based Taxonomy. *Icarus* **2002**, *158*, 146–177. [[CrossRef](#)]
70. Bodewits, D.; Villanueva, G.L.; Mumma, M.J.; Landsman, W.B.; Carter, J.A.; Read, A.M. SWIFT-UVOT Grism spectroscopy of comets: A first application TO C/2007 N3 (LULIN). *Astron. J.* **2011**, *141*, 12.
71. Bohlin, R.C. Hubble Space Telescope Spectrophotometry and Models for Solar Analogs. *Astron. J.* **2010**, *139*, 1515–1520.
72. Morgenthaler, J.P.; Harris, W.M.; Combi, M.R.; Feldman, P.D.; Weaver, H.A. Galex Fuv Observations of Comet C/2004 Q2 (Machholz): The Ionization Lifetime of Carbon. *Astrophys. J.* **2011**, *726*, 8.
73. Feldman, P.D.; Cochran, A.L.; Combi, M.R. *Spectroscopic Investigations of Fragment Species in the Coma; Comets II*; University of Arizona Press: Tucson, AZ, USA, 2004; p. 425.
74. Bodewits, D.; Bonev, B.P.; Cordiner, M.A.; Villanueva, G.L. Radiative processes as diagnostics of cometary atmospheres. *arXiv* **2022**, arXiv:2209.02616.
75. Willingale, R.; O'Brien, P.T.; Cowley, S.W.H.; Jones, G.H.; McComas, D.J.; Mason, K.O.; Osborne, J.P.; Wells, A.; Chester, M.; Hunsberger, S.; et al. Swift X-Ray Telescope Observations of the Deep Impact Collision. *Astrophys. J.* **2006**, *649*, 541–552. [[CrossRef](#)]
76. Bonamente, E.; Christian, D.J.; Xing, Z.; Venkataramani, K.; Koutroumpa, D.; Bodewits, D. Variable X-ray Emission of Comet 46P/Wirtanen. *Planet. Sci. J.* **2021**, *2*, 224. [[CrossRef](#)]
77. Cravens, T.E. Comet Hyakutake x-ray source: Charge transfer of solar wind heavy ions. *Geophys. Res. Lett.* **1997**, *24*, 105. [[CrossRef](#)]
78. Krasnopolsky, V.A. On the Nature of Soft X-Ray Radiation in Comets. *Icarus* **1997**, *128*, 368. [[CrossRef](#)]
79. Lisse, C.M.; Dennerl, K.; Englhauser, J.; Harden, M.; Marshall, F.E.; Mumma, M.J.; Petre, R.; Pye, J.P.; Ricketts, M.J.; Schmitt, J.; et al. Discovery of X-ray and Extreme Ultraviolet Emission from Comet C/Hyakutake 1996 B2. *Science* **1996**, *274*, 205–209. [[CrossRef](#)]
80. Bodewits, D.; Christian, D.J.; Torney, M.; Dryer, M.; Lisse, C.M.; Dennerl, K.; Zurbuchen, T.H.; Wolk, S.J.; Tielens, A.G.G.M.; Hoekstra, R. Spectral analysis of the Chandra comet survey. *Astron. Astrophys.* **2007**, *469*, 1183–1195. [[CrossRef](#)]
81. Krasnopolsky, V.A. CXO X-ray spectroscopy of comets and abundances of heavy ions in the solar wind. *Icarus* **2015**, *247*, 95–102. [[CrossRef](#)]
82. Kharchenko, V.; Rigazio, M.; Dalgarno, A.; Krasnopolsky, V.A. Charge Abundances of the Solar Wind Ions Inferred from Cometary X-Ray Spectra. *Astrophys. J.* **2003**, *585*, L73. [[CrossRef](#)]
83. Bodewits, D.; Juhász, Z.; Hoekstra, R.; Tielens, A.G.G.M. Catching Some Sun: Probing the Solar Wind with Cometary X-Ray and Far-Ultraviolet Emission. *Astrophys. J. Lett.* **2004**, *606*, L81–L84. [[CrossRef](#)]
84. Beiersdorfer, P.; Boyce, K.R.; Brown, G.V.; Chen, H.; Kahn, S.M.; Kelley, R.L.; May, M.; Olson, R.E.; Porter, F.S.; Stahle, C.K.; et al. Laboratory Simulation of Charge Exchange-Produced X-ray Emission from Comets. *Science* **2003**, *300*, 1558–1559. [[CrossRef](#)] [[PubMed](#)]
85. Wegmann, R.; Dennerl, K. X-ray tomography of a cometary bow shock. *Astron. Astrophys.* **2005**, *430*, L33–L36. [[CrossRef](#)]

86. Lisse, C.; Christian, D.; Dennerl, K.; Englhauser, J.; Trümper, J.; Desch, M.; Marshall, F.; Petre, R.; Snowden, S. X-Ray and Extreme Ultraviolet Emission from Comet P/Encke 1997. *Icarus* **1999**, *141*, 316–330. [[CrossRef](#)]
87. Wolk, S.J.; Lisse, C.M.; Bodewits, D.; Christian, D.J.; Dennerl, K. Chandra’s Close Encounter With The Disintegrating Comets 73p/2006 (Schwassmann-Wachmann 3) Fragment B In addition, C/1999 S4 (Linear). *Astrophys. J.* **2009**, *694*, 1293–1308.
88. Mullen, P.D.; Cumbee, R.S.; Lyons, D.; Gu, L.; Kaastra, J.; Shelton, R.L.; Stancil, P.C. Line Ratios for Solar Wind Charge Exchange with Comets. *Astrophys. J.* **2017**, *844*, 7. [[CrossRef](#)]
89. Burrows, D.N.; Hill, J.E.; Nousek, J.A.; Wells, A.A.; Short, A.D.; Willingale, R.; Citterio, O.; Chincarini, G.; Tagliaferri, G. Swift X-ray Telescope. In Proceedings of the X-ray and Gamma-Ray Instrumentation for Astronomy XI, San Diego, CA, USA, 30 July–4 August 2000; Flanagan, K.A., Siegmund, O.H., Eds.; Society of Photo-Optical Instrumentation Engineers (SPIE) Conference Series; 2000; Volume 4140, pp. 64–75. [[CrossRef](#)]
90. A’Hearn, M.F.; Belton, M.J.S.; Delamere, A.A.; Kissel, J.; Klaasen, K.P.; McFadden, L.A.; Meech, K.J.; Melosh, H.J.; Schultz, P.H.; Sunshine, J.M.; et al. Deep Impact: Excavating Comet Tempel 1. *Science* **2005**, *310*, 258–264. [[CrossRef](#)] [[PubMed](#)]
91. Mason, K.; Chester, M.; Cucchiara, A.; Gronwall, C.; Grupe, D.; Hunsberger, S.; Jones, G.; Koch, S.; Nousek, J.; O’Brien, P.; et al. Swift ultraviolet photometry of the Deep Impact encounter with Comet 9P/Tempel 1. *Icarus* **2007**, *187*, 123–131. [[CrossRef](#)]
92. A’Hearn, M.F. Deep Impact and the Origin and Evolution of Cometary Nuclei. *Space Sci. Rev.* **2008**, *138*, 237–246. [[CrossRef](#)]
93. Lisse, C.; Dennerl, K.; Christian, D.; Wolk, S.; Bodewits, D.; Zurbuchen, T.; Hansen, K.; Hoekstra, R.; Combi, M.; Fry, C.; et al. Chandra observations of Comet 9P/Tempel 1 during the Deep Impact campaign. *Icarus* **2007**, *191*, 295–309. [[CrossRef](#)]

**Disclaimer/Publisher’s Note:** The statements, opinions and data contained in all publications are solely those of the individual author(s) and contributor(s) and not of MDPI and/or the editor(s). MDPI and/or the editor(s) disclaim responsibility for any injury to people or property resulting from any ideas, methods, instructions or products referred to in the content.